Research Paper

Brain and Neuroscience Advances

Brain and Neuroscience Advances
Volume 5: 1–12

DOI: 10.1177/23982128211036332
journals.sagepub.com/home/bna
SAGE

Ratlas-LH: An MRI template of the Lister hooded rat brain with stereotaxic coordinates for neurosurgical implantations

Malcolm J. W. Prior[1], Tobias Bast[2], Stephanie McGarrity[3], Jürgen Goldschmidt[4], Daniel Vincenz[4], Adam Seaton[3], Gerard Hall[5] and Alain Pitiot[6,7]

Abstract

There is currently no brain atlas available to specifically determine stereotaxic coordinates for neurosurgery in Lister hooded rats despite the popularity of this strain for behavioural neuroscience studies in the United Kingdom and elsewhere. We have created a dataset, which we refer to as 'Ratlas-LH' (for Lister hooded). Ratlas-LH combines in vivo magnetic resonance images of the brain of young adult male Lister hooded rats with ex vivo micro-computed tomography images of the ex vivo skull, as well as a set of delineations of brain regions, adapted from the Waxholm Space Atlas of the Sprague Dawley Rat Brain. Ratlas-LH was produced with an isotropic resolution of 0.15 mm. It has been labelled in such a way as to provide a stereotaxic coordinate system for the determination of distances relative to the skull landmark of bregma. We have demonstrated that the atlas can be used to determine stereotaxic coordinates to accurately target brain regions in the Lister hooded rat brain. Ratlas-LH is freely available to facilitate neurosurgical procedures in the Lister hooded rat.

Keywords

Stereotaxic, brain template, Lister hooded rat, MRI

Received: 23 December 2019; accepted: 13 July 2021

Introduction

Stereotaxic coordinates for the implantation of devices into specific regions of the rat brain are typically determined with the aid of an atlas using the coordinate system introduced by Paxinos and Watson (1982). This coordinate system has been used in the atlas created by Paxinos and Watson, now in its seventh edition (Paxinos and Watson, 2013), and Swanson, which is now in its fourth edition and is freely available online (Swanson, 2018). These established atlases, which have been carefully constructed from detailed histological data, have long been the authoritative guide to the identification of formations and microscopic structures within the rat brain. However, it has been our experience that stereotaxic coordinates derived from these atlases were of limited accuracy when used to surgically target brain regions in Lister hooded rats; a strain that is widely used in behavioural neuroscience studies, particularly in the United Kingdom.

This limited accuracy likely reflects discrepancies between the atlas and the brain in vivo. These discrepancies could be due to distortions of the fixed material used to create the histological atlases (for detailed discussion, see Simmons and Swanson, 2009), or possible morphological differences between the strain used to create the atlas and the Lister hooded rat used in our neurosurgical procedures. However, Swanson (2018) suggested that there is very little shrinkage of the histological material during the preparation of slides using the methods of Paxinos and Watson (1986), hence the fairly universal acceptance of the coordinate system of Paxinos and Watson (1986) even in the atlas by Swanson (2018). Paxinos et al. (1985) examined possible errors in coordinate values when using an atlas created from male

[1]School of Medicine and Neuroscience at Nottingham, University of Nottingham, Nottingham, UK
[2]School of Psychology and Neuroscience at Nottingham, University of Nottingham, Nottingham, UK
[3]School of Psychology, University of Nottingham, Nottingham, UK
[4]Department of Systems Physiology of Learning, Leibniz Institute for Neurobiology, Magdeburg, Germany
[5]School of Life Sciences, University of Nottingham, Nottingham, UK
[6]Laboratory of Image & Data Analysis, Ilixa Ltd., London, UK
[7]Ludwig Boltzmann Institute for Experimental and Clinical Traumatology, Vienna, Austria

Corresponding authors:
Malcolm J. W. Prior, School of Medicine and Neuroscience at Nottingham, University of Nottingham, Nottingham NG7 2UH, UK.
Email: malcolm.prior@nottingham.ac.uk

Tobias Bast, School of Psychology and Neuroscience at Nottingham, University of Nottingham, University Park, Nottingham NG7 2RD, UK.
Email: tobias.bast@nottingham.ac.uk

Wistar rats (Paxinos and Watson, 1982) to determine stereotaxic coordinates in female Wistar, male Long-Evans or male Sprague-Dawley rats. They reported only small differences between rat strains in the anterior-posterior distance between bregma and either the nucleus accumbens or the descending limb of the seventh nerve. However, we found that we reached an area in the ventral hippocampus corresponding to a coronal section of about 6 mm posterior to bregma in the atlas by Paxinos and Watson (2013) by using an anterior-posterior coordinate of 5 mm posterior to bregma in Lister hooded rats (McGarrity et al., 2017).

It is possible to create a brain template from in vivo magnetic resonance imaging (MRI) data that can be used to provide stereotaxic coordinates. This has the advantage that the data obtained reflects the dimensions of the brain in vivo and data can be obtained from a relevant sex, age group and strain. Although the resolution of in vivo MRI data is much lower than that of histological sections, it can be detailed enough to provide images for the derivation of stereotaxic coordinates. A number of in vivo MRI atlases are available online (Hess et al., 2018), though we have not been able to find any for the Lister hooded rat. Here, we used MRI of the brain and micro-computed tomography (micro-CT) of the skull to create a template of the Lister hooded rat brain to provide stereotaxic coordinates that may be used for neurosurgery. The MRI protocol was adapted to allow the collection of in vivo super-resolution images (Irani and Peleg, 1990; Pitiot et al., 2007) of the Lister hooded rat brain with an isotropic resolution of 0.15 mm within an acceptable time frame of 1.5 h of scanning for each rat. In vivo MRI image data from the brains of seven young adult male Lister hooded rats were combined to create an anatomical average image of the brain. Data from ex vivo micro-CT were similarly used to create an anatomical average of the skull, which was combined with the MRI data to create a single template. We also included a set of atlas delineations of brain regions, which we adapted from the Waxholm Space (WHS) Atlas of the Sprague Dawley Rat Brain (Kjonigsen et al., 2015; Osen et al., 2019; Papp et al., 2014). This dataset, which we refer to as 'Ratlas-LH' (for Lister hooded), can be viewed using freely available software and can provide stereotaxic coordinates for neurosurgery in Lister hooded rats. This article also includes an assessment of the validity of using the template to derive stereotaxic coordinates, based on intracerebral implantations of microinfusion cannulae in the Lister hooded rat.

Methods

Animals

Seven adult male Lister hooded rats (Charles River, UK) with an average weight (± SD) of 332 ± 5 g (about 2–3 months old) were used to create the template. Seven rats were used to allow the creation of an anatomical average brain image, which would have a superior signal-to-noise ratio (SNR) compared to data obtained from a single rat. The rats were housed in groups of up to four per cage under temperature- and humidity-controlled (21°C ± 0.5°C and 50% ± 8%) conditions with an alternating 12-h light and dark cycle. They had ad libitum access to food and water. The in vivo work to create the MRI template was conducted in accordance with the requirements of the United Kingdom Animals (Scientific Procedures) Act 1986 and under the authority of Project Licence number 40/3454.

Preparation of rats for MRI

Following induction of anaesthesia with 5% isoflurane in a 2:1 mixture of N_2O and carbogen (95% oxygen, 5% CO_2) in a chamber, anaesthesia was maintained throughout the procedure using isoflurane in the range of 2% to 1.5% in the same gas mixture. Rats were transferred to a cradle and fixed into place using ear bars and an incisor bar. Body temperature was maintained using a homeothermic blanket with a rectal temperature probe (Harvard Apparatus, UK).

In vivo acquisition of MRI data for super-resolution brain images

The cradle containing the rat was transferred into the magnet for imaging. Body temperature and breathing rate were recorded and maintained throughout imaging. Body temperature was kept at 37.5°C° ± 1.0°C by adjusting the temperature of water circulated through the cradle, and the breathing rate was maintained at around 50 ± 10 breathes per min by adjusting the isofluorane levels.

Imaging was performed using a Bruker Biospec 7T system with a 30 cm bore magnet and 12 cm internal bore gradients supplying 0.4 Tesla metre^{-1} (Bruker Biospin, Ettlingen, Germany). MRI data were acquired with a 4-channel receive-only phased array coil placed over the rat head; a 72 mm volume coil was used for excitation.

Scout images were acquired with 30 slices in three orthogonal directions using fast spin-echo imaging (Hennig et al., 1986) with the following parameters: echo train length = 8 echoes (echo spacing of 11.8 ms), $TE_{effective}$ = 23.6 ms, TR = 5000 ms, slice thickness = 1 mm; in plane resolution was 0.125 mm × 0.125 mm for coronal images, whereas images with dorso-ventral and sagittal views were acquired at 0.125 mm × 0.141 mm resolution. These images were then used to position sagittal slices for the acquisition of the template data. Alignment of the template slices with the brain anatomy in the dorso-ventral, sagittal and coronal directions was optimised to ensure that the brain, including the olfactory bulb and cerebellum, was within the acquisition field of view (FOV).

Images for the template were acquired using fast spin-echo imaging (Hennig et al., 1986) with an echo train length of 8 echoes (echo spacing = 12.8 ms), $TE_{effective}$ = 25.6 ms, TR = 7503.4 ms and 16 signal averages. The number of data points collected were 106 × 188 over a slice FOV of 15.9 mm × 28.2 mm, giving an in-plane resolution of 0.15 mm. In order to use a FOV that was smaller than the head of the rat, and smaller than the detection volume of the coil, it was necessary to use five saturation bands strategically placed around the brain carefully aligned with the edge of the imaging FOV. Saturation band positions and dimensions were as follows: one band of 15 mm thickness in the dorso-ventral plane below the brain, two bands of 8 mm thickness in the sagittal plane placed laterally, one axial band of 10 mm thickness in front and a second of 15 mm thickness behind the brain.

Datasets were obtained using the slice package feature of Paravision 5 (Bruker, Ettlingen, Germany) to divide each imaging protocol into two slice packages with dimensions listed above with slices aligned in the sagittal plane. Each slice package was acquired with 0.3 mm slice thickness with a 0.3 mm gap between slices; the slice packages were arranged such that the slices of

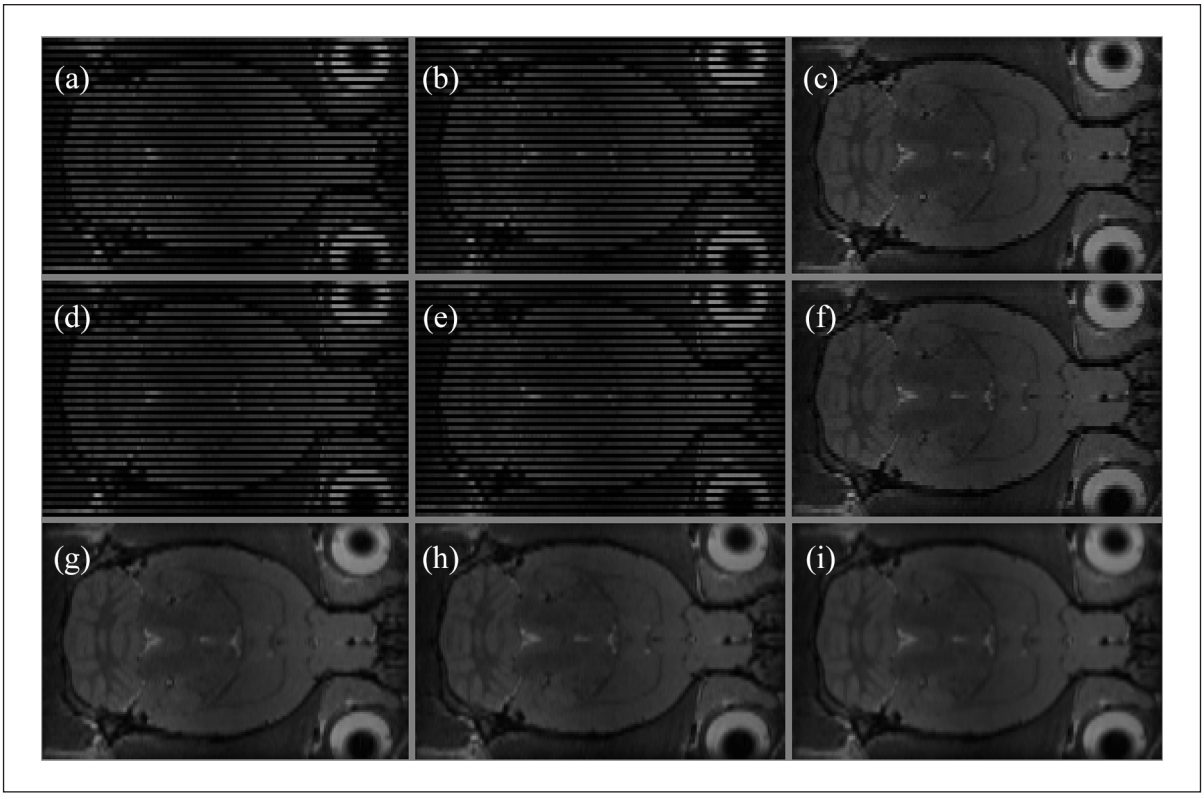

Figure 1. The acquisition of interleaved MRI datasets and the reconstruction of super-resolution magnetic resonance image volumes: (a) and (b) interleaved slice positions for acquisition of two corresponding slice packages containing 0.3-mm-thick slices with 0.3 mm gaps between slices. (c) Image volume with corresponding slice packages combined from (a) and (b). (d) and (e) interleaved slice positions for acquisition of two corresponding slice packages with slices positions offset by 0.15 mm from the slice positions in (a) and (b), respectively. (f) Image volume with corresponding slice packages combined from (d) and (e). (g) and (h) image volumes created from (c) and (f) using interpolation to create 0.15 mm slices. (i) A super-resolution image volume following the addition of image volumes shown in (g) and (h).

one package were acquired where there was a gap in the corresponding slice package (Figure 1(a) and (b)). The complete image volume (Figure 1(c)) consists of the interlaced data from the corresponding slice packages (Figure 1(a) and (b)). Furthermore, a second image volume was acquired (Figure 1(f)) that also consisted of two slice packages (Figure 1(d) and (e)). However, the image volumes shown in Figure 1(c) and (f) were offset by 0.15 mm from each other in the slice direction, which facilitated the acquisition of data for the reconstruction of super-resolution images with a final isotropic resolution of 0.15 mm (Figure 1(i)). The acquisition time for each of the two pairs of slice packages was 46 min, resulting in a total acquisition time of 92 min for the template data from each rat. Following acquisition of in vivo data, the rats were terminally anaesthetised with an overdose of pentobarbital and transcardially perfused with phosphate-buffered saline, followed by 4% paraformaldehyde solution, to preserve the heads.

Ex vivo acquisition of micro-CT skull data

The external tissues of the head were removed leaving the brain inside the skull for CT imaging. Micro-CT images were obtained with an isotropic resolution of 40 µm. Measurements were made with a GE eXplore Locus CT at 70 kVp, 450 µA, with 1200 projections of 200 ms exposure time and two averages. No calibration phantoms for Hounsfield-unit calibration were used.

Magnetic resonance and micro-CT image reconstruction and processing

Magnetic resonance data was transformed into 32-bit images in Bruker image format. Images in slice packages were automatically reconstructed from each pair of interleaved slice packages by use of the 3D Jive image analysis software provided in Paravision 5 (Bruker, Ettlingen, Germany) to create image volumes represented in Figure 1(c) and (f). The resulting datasets containing 60 slices of 0.3 mm thickness were interpolated using 3D Jive to increase the number of slices to 120 with a slice thickness of 0.15 mm in both image volumes obtained from each rat (Figure 1(g) and (h)). All magnetic resonance images were then converted into NIFTI format using Fiji (Rasband, W.S., ImageJ, U. S. National Institutes of Health, Bethesda, Maryland, USA, https://imagej.nih.gov/ij/, 1997–2018).

The super-resolution images were constructed by the addition of corresponding pairs of image volumes (Figure 1(g) and (h)) to create a single image dataset from each rat (Figure 1(i)); this addition was carried out using FSL (https://fsl.fmrib.ox.ac.uk/fsl/fslwiki; Jenkinson et al., 2012). Super-resolution images were

processed to correct for signal bias due to the use of a surface coil for data acquisition using FSL (Zhang et al., 2001). An image mask of the brain was generated for each super-resolution image volume using the active contour segmentation process in ITK-SNAP (http://www.itksnap.org, Yushkevich et al., 2006). However, this automated process did not segment the brain with sufficient accuracy for our purposes and manual adjustment of the mask was required to create an accurate segmentation. Brain image data was then extracted from the super-resolution images using FSL.

DICOM images obtained from micro-CT imaging were converted into NIFTI data sets using MIPAV (Medical Image Processing, Analysis, and Visualization) application (https://mipav.cit.nih.gov/index.php).

Template construction

All brain magnetic resonance images were registered to a chosen reference image using a rigid body transformation (6 degrees of freedom) using FSL FLIRT (https://fsl.fmrib.ox.ac.uk/fsl/fslwiki/FLIRT; Jenkinson et al., 2002; Jenkinson and Smith, 2001). The reference image was chosen by selecting the MRI dataset where the brain most matched the 'flat skull' position used in the stereotaxic coordinate system of Paxinos and Watson (1986). Brain images were then processed using Advanced Normalization Tools (ANTs) obtained from stnava.github.io/ANTs/ (Avants and Gee, 2004). Template registration was performed using the script antsMultivariateTemplateConstruction.sh (Avants et al., 2011) from the ANTs toolbox to create an anatomical average image. The anatomical average image was then oversampled (to an isotropic resolution of 0.075 mm) to produce a smooth image when it is used in the viewing software for the derivation of stereotaxic coordinates.

Micro-CT images were registered to a chosen reference skull image using a rigid body transformation (6 degrees of freedom) within FSL FLIRT. Skull images were then processed using ANTs template registration function (antsMultivariateTemplateConstruction.sh, Avants et al., 2011) to create an anatomical average image (skull template). Five out of seven skull images were used in the construction of the skull template because two of the micro-CT images did not contain complete skull data.

Finally, the MRI brain and micro-CT skull templates were aligned. To facilitate this, the cranial cavity was segmented using the automatic segmentation process of ITK-SNAP to produce a volume image of the inside of the skull that had the same resolution, orientation and field-of-view as the CT data. The segmentation volume from the automatic process required a small amount of manual adjustment to accurately reflect the inside of the skull. The segmented image volume of the inside of the skull was then aligned with the MRI template image using a rigid body transformation (6 degrees of freedom) within FSL FLIRT and the transformation matrix was saved. This saved matrix was then applied to the skull template, also using FSL FLIRT, to align it with the brain template before these two images were added together using FSL maths.

Addition of atlas delineations

We also included a set of delineations of brain regions in the Ratlas-LH package to assist in the process of determining stereotaxic coordinates. These delineations were adapted from the WHS Atlas of the Sprague Dawley Rat Brain (Kjonigsen et al., 2015; Osen et al., 2019; Papp et al., 2014 see also https://www.nitrc.org/projects/whs-sd-atlas/). They are available in an electronic, contiguous 3D format that covers the entire rat brain. The WHS T2* Sprague Dawley image dataset, the WHS brain mask, and version 3 of the atlas delineations and labels for the Sprague-Dawley rat were obtained from https://www.nitrc.org/frs/?group_id=1081&release_id=4070.

In order to adapt the atlas delineations for use with Ratlas-LH, we first required a new mask for the extraction of the WHS brain. This mask was specifically made to extract the WHS brain along with some non-brain tissue and cerebrospinal fluid (CSF) from outside of the brain such that the contents of the extracted WHS image were similar to that found in the Ratlas-LH brain template. The mask for the extraction of an extended area of the WHS brain was constructed by adapting the WHS atlas delineations to form a mask. ITK-SNAP was used to add a new segmentation layer to the WHS delineations that included areas of non-brain tissues and CSF similar to those included in the Ratlas-LH brain template. This extended set of WHS delineations was then converted to a binary mask using MIPAV and used to extract a brain image from the WHS Sprague Dawley dataset using FSL.

The WHS delineations were adapted for use in Ratlas-LH using the WHS Sprague Dawley brain that was extracted as described above. The Ratlas-LH brain template (without skull data) was then registered to the extracted WHS brain using the script antsRegistrationSyN.sh available in ANTs (Avants et al., 2011). The inverse transformation matrix from this process was then applied to the WHS atlas delineations image, using antsApplyTransforms, to align them with the anatomy of Ratlas-LH. To display views of the delineations overlaid on Ratlas-LH, we used ITK-SNAP.

Implementation and use of the coordinate system

The position of bregma was assigned to the coordinate system of the final template. The correct position of bregma in the anterior-posterior and lateral directions of the brain was confirmed by reference to the alignment of this position with the crossing point of the anterior commissure at the midline of the brain (Paxinos et al., 1985). The dorso-ventral position of bregma was assigned to the surface of the skull directly above the midline point of the crossing of the anterior commissure. This assigned position of bregma corresponded to the position of bregma indicated by the skull CT data of Ratlas-LH.

The completed template image dataset is in NIFTI format. The stereotaxic coordinates for bregma (anterior-posterior = 0, lateral = 0, dorso-ventral = 0 mm) were set in the world coordinate values.

The stereotaxic coordinates in Ratlas-LH can be found by using one of several applications. We have used the free image display software MIPAV with Ratlas-LH (without the atlas delineations) to determine stereotaxic coordinates for our neurosurgical procedures in Lister hooded rats. This process was assisted by reference to the atlases of Paxinos and Watson (1998) and Swanson (2004) to provide more detail of the rat neuroanatomy in the region of interest beyond the apparent white matter and grey matter regions that are displayed in the T2-weighted magnetic resonance images of Ratlas-LH. A guide to using MIPAV to obtain stereotaxic coordinates is included in the supplementary

information and further details of the process used to determine stereotaxic coordinates for neurosurgery in our studies are described below (see *Ratlas-LH validation: stereotaxic cannula implants using Ratlas-LH coordinates*). For readers who wish to make use of the atlas delineations and their labels, we recommend the use of ITK-SNAP to display and find coordinates in Ratlas-LH. A guide to using Ratlas-LH with the WHS Atlas delineations is included in the supplementary material.

Ratlas-LH validation 1: stereotaxic cannula implants using Ratlas-LH coordinates

To demonstrate the use and validity of the in vivo MRI template of the Lister hooded rat brain, we report on the accuracy of cannula implants into the intermediate hippocampus and the medial nucleus accumbens that we completed as part of two microinfusion studies (for preliminary reports of these studies, please see: McGarrity et al., 2015; Seaton, 2019).

A five-stage process was used to find the correct coordinate values for our implantations in the Lister hooded rat:

1. We found our region of interest in the atlas of Paxinos and Watson (1998) and noted the coordinate values for the Wistar rat.
2. We then observed and noted the landmark features of the brain relative to the region of interest as displayed in Paxinos and Watson (1998). These landmark features included the outline shape of the brain, the position and shape of ventricle regions, the shape and position of major white matter regions, and the shape and position of grey matter regions.
3. The coordinate values for our region of interest obtained from Paxinos and Watson (1998) in stage 1 were then used to place the crosshair cursors in MIPAV (Medical Image Processing, Analysis, and Visualization, https://mipav.cit.nih.gov/index.php) that was displaying the Ratlas-LH. This was achieved by entering the coordinate values into the relevant windows of the Scanner RAS coordinates tab in the Tri-planar view display.
4. An adjustment was then made to the crosshair cursor positions in MIPAV to place them in the correct region of interest, making sure that they indicate the same position relative to the 3D landmark features of the brain noted in step 2 above.
5. The correct coordinates for use in the implantation of micro-cannulae into the Lister hooded rat brain were then read from the Scanner RAS coordinates tab in the Tri-planar view display of MIPAV.

In the 'Results' section, we report on the accuracy of the implantations using the stereotaxic coordinates derived from our MRI template of the Lister Hooded rat brain. The two studies used adult male Lister hooded rats (Charles River, UK), aged 2–3 months and housed as described for the rats used for template construction. All work was conducted in accordance with the requirements of the United Kingdom Animals (Scientific Procedures) Act 1986, and under the authority of Project Licence number 40/3454 and 30/3357. Using surgical procedures as described previously (McGarrity et al., 2017; Pezze et al., 2014) and coordinates obtained from the Ratlas-LH brain template, rats were stereotaxically implanted with guide cannula aimed above the medial nucleus accumbens (n = 16) and the intermediate hippocampus (n = 10). The guide cannulae (stainless steel, 26-gauge, held in a plastic pedestal; Plastics One, Bilaney, UK) were filled with stylets (stainless steel, 33 gauge; Plastic Ones), which protruded 0.5 mm from the guides. For intracerebral infusions, the stylets would be replaced by infusion cannulae (stainless steel, 33 gauge; Plastic Ones), which also protruded 0.5 mm from the guides. The target coordinates for the tips of the stylets and infusion cannulae in the intermediate hippocampus were −4.7 mm anterior, ±4.3 mm lateral, relative to bregma, and −3.0 mm ventral from dura; the dura was taken to be at the upper surface of the brain in the template. The target coordinates for stylets/infusion cannula tips in the medial nucleus accumbens were 1.5 anterior, ±1.0 mm lateral, relative to bregma, and −7.2 mm ventral from the skull. As skull data had not yet been included in the Ratlas-LH template when these cannula implants were performed, we measured the ventral distance from the top of the brain to the region of interest in the template and added 0.5 mm to this distance to take into account the thickness of the skull.

After these rats had completed experiments combining intracerebral drug microinfusions with behavioural testing, the rats were transcardially perfused with saline, followed by 4% paraformaldehyde solution, under terminal anaesthesia (overdose of pentobarbital), brains were extracted from the skull and stored in 4% paraformaldehyde solution and processed for verification of cannula placements, using standard histological procedures as described previously (McGarrity et al., 2017; Pezze et al., 2014). Brains were cut into 80 μm coronal sections on a vibratome, which were mounted on slides and stained with cresyl violet. In the 'Results' section, we present photographs of histology slides showing exemplar cannula placements. In addition, we determined the cannula placements in all rats using a light microscope and mapped them onto coronal sections of the rat brain stereotaxic atlas by Paxinos and Watson (1998). These data are presented to show the range of positions achieved using the coordinates.

Ratlas-LH validation 2: comparison of Ratlas-LH coordinates with coordinates used in a previous study

We examined stereotaxic coordinates for the ventral hippocampus from a previous publication (McGarrity et al., 2017) to see if they agree with coordinate values obtained from Ratlas-LH. The coordinates for the ventral hippocampus used in McGarrity et al. (2017) were not derived from Ratlas-LH but were obtained by a series of pilot surgeries implanting guide cannulae. In the 'Results' section, we compare the cannula placements in McGarrity et al. (2017) with the position that the coordinates indicate in Ratlas-LH. We present a photograph of a histological slide showing an exemplar cannula placement and mappings of placements across rats to show the range of positions achieved using the coordinates. These are compared to the relevant section of Ratlas-LH at the location given by the same coordinate values.

Results

Ratlas-LH construction

Examination of the super-resolution images from each rat revealed good quality images of the rat brain (Figure

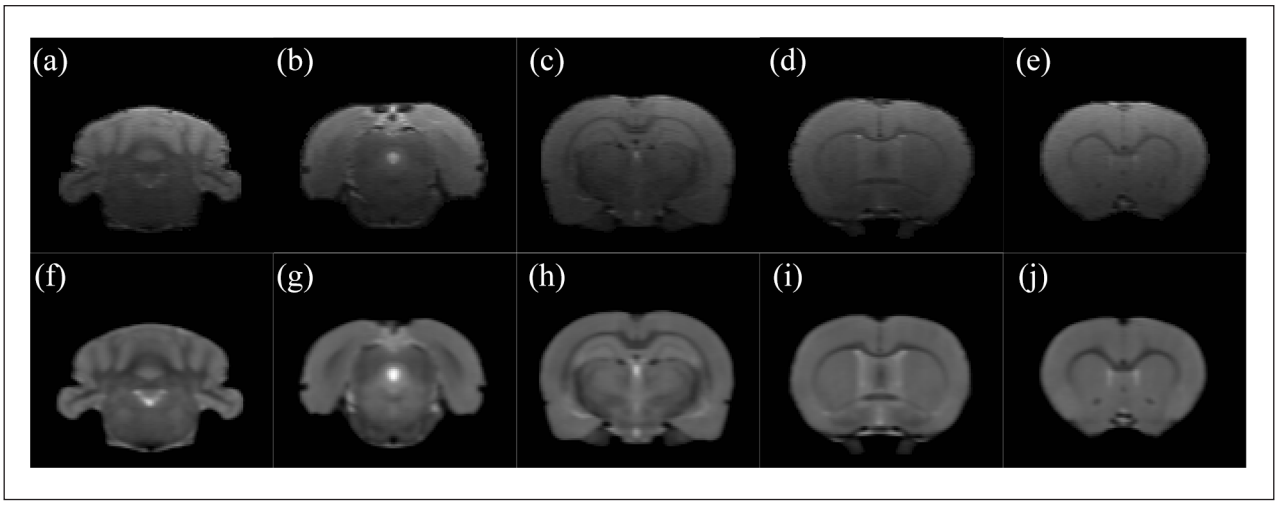

Figure 2. Super-resolution images from a single rat (upper row) compared to images from an average anatomical dataset (lower row) created from seven rats. Note the substantially less 'grainy' appearance and clarity, reflecting improved signal-to-noise ratio, in the images averaged across seven rats compared to the images from one single rat. Coronal sections through the cerebellum at the level of the paraflocculus (a, f), sections at the level of lambda (b, g), sections displaying the dorsal/septal part of the hippocampus (c, h), sections displaying posterior parts of the striatum at the level of bregma, above the crossing point of the anterior commissure (d, i), and sections showing more anterior parts of the striatum, including the ventral striatum/nucleus accumbens surrounding the anterior commissure (which appears in very dark grey) (e, j).

2(a)–(e)). Super-resolution MRI data from seven rats were combined into an anatomical average template, which resulted in an image volume with superior SNR compared to the single rat volume dataset (Figure 2). Data from micro-CT were also combined to produce an anatomical average template. The Ratlas-LH template was completed by the fusion of the MRI brain template and micro-CT skull template images into a single image volume (Figure 3). A representative selection of atlas delineations is presented in Figure 4, using the same locations in Ratlas-LH as displayed in Figure 3 for comparison purposes. The Ratlas-LH along with the delineations and their labels are available for free download (https://www.nitrc.org/projects/ratlas-lham). The Ratlas-LH template can be viewed in various medical imaging software packages. We have used MIPAV and we have included a guide to using this free software to obtain stereotaxic coordinates in the supplementary material. In order to make use of the atlas delineations, we recommend the use of ITK-SNAP. A guide to using ITK-SNAP for the derivation of stereotaxic coordinates is also provided in the supplementary material.

Ratlas-LH validation 1: stereotaxic cannula implants using Ratlas-LH coordinate

We used Ratlas-LH to determine stereotaxic coordinates for the implantation of infusion cannulae in the intermediate hippocampus and the medial nucleus accumbens of Lister hooded rats as part of two drug microinfusion studies in our lab (papers in preparation). The target coordinates derived from Ratlas-LH for the intermediate hippocampus were 4.7 mm posterior and ±4.3 mm lateral to bregma, and −3.0 mm ventral from dura. The coordinates for the medial nucleus accumbens were 1.5 mm anterior, ±1 mm lateral and −7.2 mm ventral from bregma. The position of these coordinates in Ratlas-LH, as displayed in MIPAV, is indicated by the crosshairs shown in Figure 5(a) for the intermediate hippocampus and in Figure 6(a) for the medial nucleus accumbens. The accuracy of the infusion cannulae placements in the target region was verified by histological sections, an example of which is shown in Figure 5(b) for the intermediate hippocampus and in Figure 6(b) for the medial nucleus accumbens. In these studies, 10 rats were bilaterally implanted for microinfusions into the intermediate hippocampus and 16 rats for infusion into the medial nucleus accumbens. The ranges of infusion cannula tip placements across rats that were achieved in the intermediate hippocampus and the medial nucleus accumbens are shown in Figures 5(c) and 6(c), respectively.

Ratlas-LH validation 2: comparison of Ratlas-LH coordinates with coordinates used in a previous study

We also examined histological findings from our previous study (McGarrity et al., 2017) where Lister hooded rats were implanted with cannulae into the ventral hippocampus using stereotaxic coordinates based on pilot surgeries. These data provide us with the opportunity to examine the accuracy of the coordinate system in Ratlas-LH from a complementary approach to that described in the section *Ratlas-LH validation 1*, above. We know from this published work (McGarrity et al., 2017) that the coordinate values of 5.2 mm posterior to bregma, ±4.8 mm lateral from midline and 6.5 mm ventral from dura result in the accurate positioning of cannulae into the ventral hippocampus in the Lister hooded rat. Here we compare the data for the cannula placements with the location of these coordinates in Ratlas-LH.

The target position that was given by the coordinates used in McGarrity et al. (2017) was located in Ratlas-LH. This position is shown by the crosshairs in Figure 7(a), which indicated a

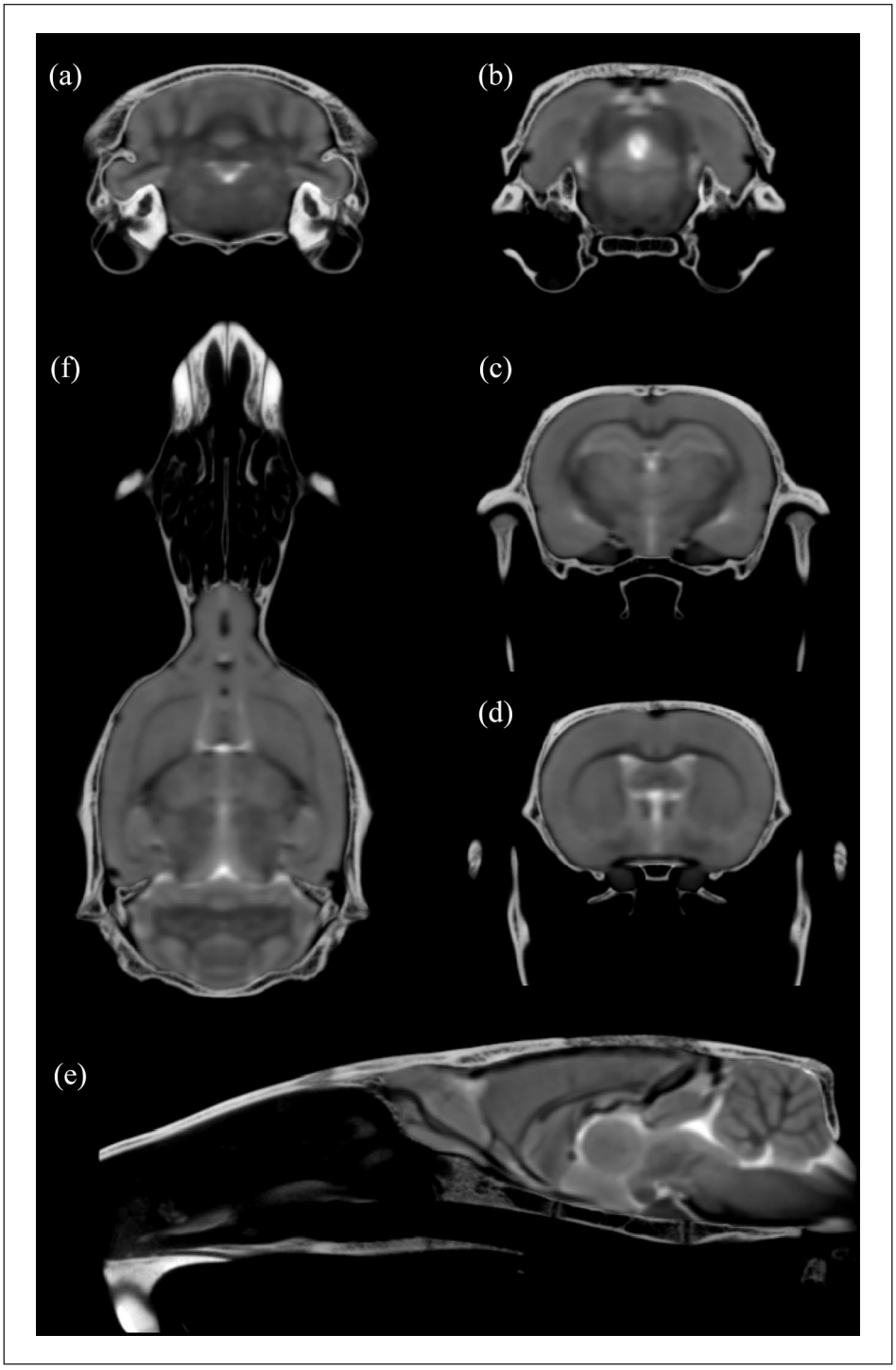

Figure 3. Selected views taken from the completed atlas including in vivo magnetic resonance images of the brain surrounded by ex vivo micro-CT images of the skull. (a) to (d) Coronal views at positions –10.5 mm, –7.6 mm, –3.0 mm and –0.45 mm posterior to bregma, respectively. (e) Sagittal view of the midline of the brain. (f) Dorso-ventral view at –5.7 mm inferior to bregma.

position in the ventral hippocampus. The accuracy of the infusion cannulae placements in the target region was verified by histological sections, an example of which is shown in Figure 7(b) (reproduced from McGarrity et al., 2017). Data showing the range of cannula placements using these coordinates in the Lister hooded rat are shown in Figure 7(c). The comparison of these data revealed excellent correspondence between the coordinates in Ratlas-LH and the actual cannula placements in the Lister hooded rat brain, further supporting the in vivo accuracy of the coordinate system in Ratlas-LH.

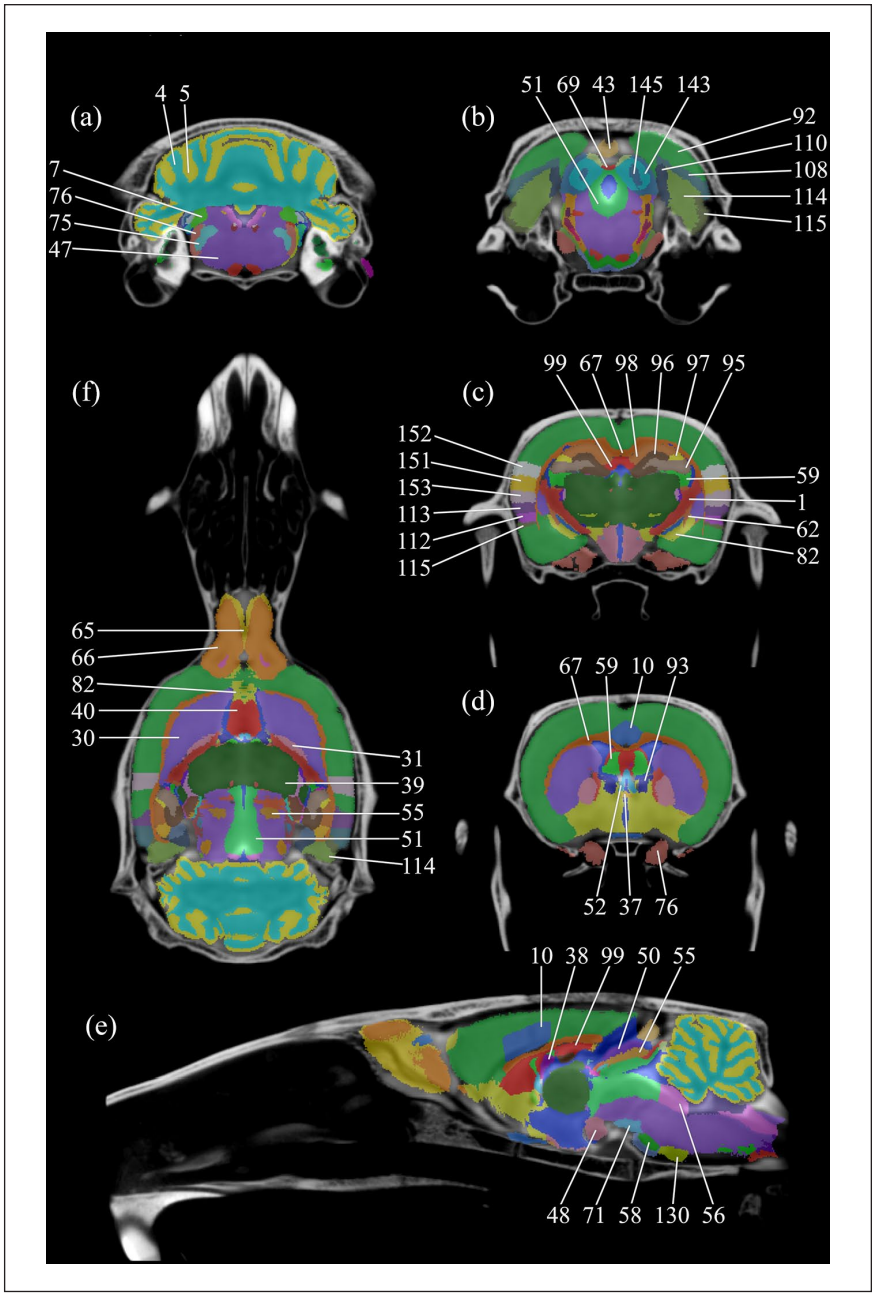

Figure 4. Selected views taken from the completed atlas showing the atlas delineations overlaid on the in vivo magnetic resonance images of the brain surrounded by ex vivo micro-CT images of the skull: (a) to (d) Coronal views at positions –10.5 mm, –7.5 mm, –3.0 mm and –0.45 mm posterior to bregma, respectively. (e) Sagittal view of the midline of the brain. (f) Dorso-ventral view at –5.7 mm inferior to bregma. Brain areas are labelled with their brain region numbers as listed in version 3 of the WHS atlas (https://www.nitrc.org/projects/whs-sd-atlas/). Area labels are as follows: 1 descending corticofugal pathways, 4 molecular layer of the cerebellum 5 granule cell level of the cerebellum, 7 inferior cerebellar peduncle, 10 cingulate cortex, area 2, 30 striatum, 31 globus pallidus, 37 anterior commissure, posterior part, 38 ventral hippocampal commissure, 39 thalamus, 40 septal region, 43 pineal gland, 47 brainstem, 48 hypothalamic region, 50 superficial grey layer of the superior colliculus, 51 periaqueductal grey, 52 fornix, 55 deeper layers of the superior colliculus, 56 periventricular grey, 58 pontine nuclei, 59 fimbria of the hippocampus, 62 stria terminalis, 65 glomerular layer of the olfactory bulb, 66 olfactory bulb, 67 corpus callosum and associated subcortical white matter, 69 inferior colliculus, commissure, 71 interpeduncular nucleus, 75 spinal trigeminal nucleus, 76 spinal trigeminal tract, 82 basal forebrain region, 92 neocortex, 93 bed nucleus of the stria terminalis, 95 cornu ammonis 3, 96 dentate gyrus, 97 cornu ammonis 2, 98 cornu ammonis 1, 99 fasciola cinereum, 108 postrhinal cortex, 110 parasubiculum, 112 perirhinal area 35, 113 perirhinal area 36, 114 entorhinal cortex, 115 lateral entorhinal cortex, 130 trapezoid body, 143 inferior colliculus, central nucleus, 145 inferior colliculus, external cortex, 151 primary auditory cortex, 152 secondary auditory cortex, dorsal area, 153 secondary auditory cortex, ventral area.

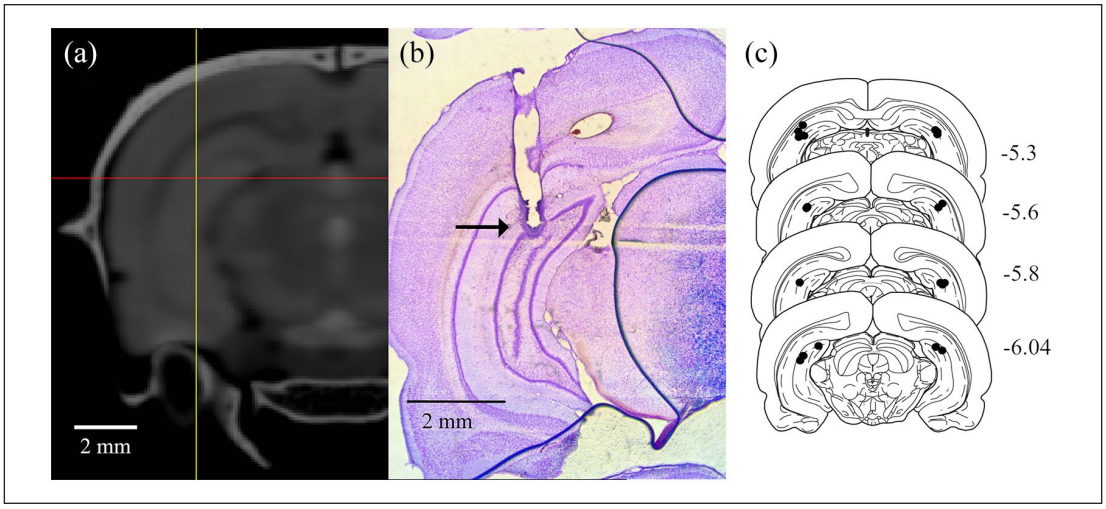

Figure 5. Coordinate positions in Ratlas-LH and microinfusion cannula placement in the intermediate hippocampus: (a) The position of the coordinates in Ratlas-LH (indicated by the red and yellow crosshairs in the image) that were used as target coordinates for stereotaxic surgery. (b) A photomicrograph showing an example placement of an infusion cannula tip in the intermediate hippocampus; the infusion site (arrow) is marked by a dark area of gliosis, with a track left by the guide cannula visible above. (c) Spread of locations of infusion cannula tips (dots) across 10 rats that received cannula implants targeting the intermediate hippocampus. Locations are shown on coronal plates adapted from Paxinos and Watson (1998). Numbers indicate the distance (in mm) from bregma in the Paxinos and Watson (1998) coordinates system.

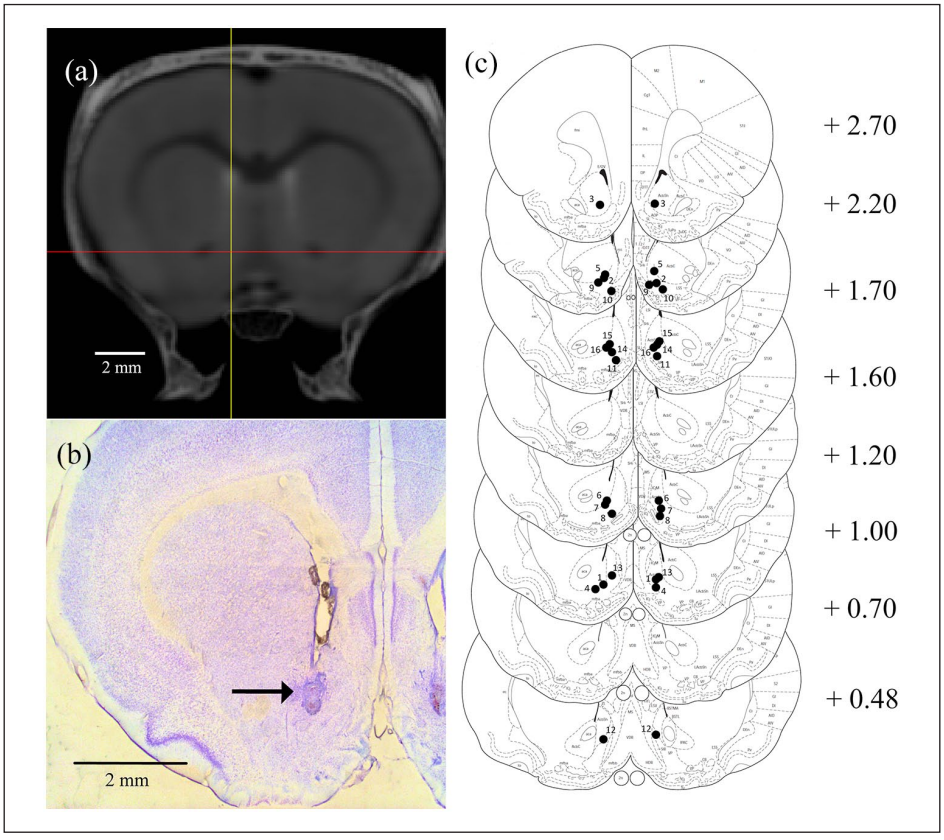

Figure 6. Coordinate positions in Ratlas-LH and microinfusion cannula placement in the medial nucleus accumbens: (a) The position of the coordinates in Ratlas-LH (indicated by the red and yellow crosshairs in the image) that were used as target coordinates for stereotaxic surgery. (b) A photomicrograph showing an example placement of an infusion cannula tip in the medial nucleus accumbens; the infusion site (arrow) is marked by a dark area of gliosis, with a track left by the guide cannula visible above. (c) Spread of locations of infusion cannula tips (dots) across 16 rats that received cannula implants targeting the medial nucleus accumbens. Locations are shown on coronal plates adapted from Paxinos and Watson (1998). Numbers indicate the distance (in mm) from bregma in the Paxinos and Watson (1998) coordinates system.

Discussion

We have developed Ratlas-LH, a new freely available in vivo MRI template of the adult male Lister hooded rat brain co-registered with ex vivo micro-CT images of the skull. A set of delineations of brain regions adapted from the WHS Sprague Dawley rat atlas (Kjonigsen et al., 2015; Osen et al., 2019; Papp et al., 2014) have been included to assist in the derivation of coordinate values. In addition, we demonstrated that the Ratlas-LH system can be used to determine accurate stereotaxic coordinates for neurosurgical procedures in the Lister hooded rat and that stereotaxic coordinates from a previous study in the Lister hooded rat (McGarrity et al., 2017) are in agreement with the coordinate system of Ratlas-LH.

Data acquisition strategy

Data acquisition and reconstruction strategies were implemented to provide magnetic resonance images with an isotropic resolution of 0.15 mm in an acceptable scan time (1.5 h) for each rat given the limitations of the intrinsic SNR of MRI and working with the available equipment. In order to achieve this goal, the acquisition was facilitated by (1) the division of the acquisition scheme into slice packages to facilitate the acquisition of 0.3-mm-thick image slices to cover the whole brain; (2) the use of a four-coil arrayed head coil, in combination with a actively decoupled volume excitation coil to provide improved SNR over and better coverage of the brain compared to using a standard surface coil; and (3) limiting the field-of-view of the data acquisition to the cranial area only by use of saturation bands.

There were a number of constraints that prevented us from acquiring data using a less complex acquisition scheme. The acquisition of super-resolution images without using the saturation bands (with a FOV of 35 mm × 50 mm and with 0.3 mm slices) would have taken 4.37 h per rat due to the requirement for a long repetition time in order to remain within the duty cycle of the gradients. Similarly, the duty cycle of the gradients imposed limits on the repetition time for the acquisition of other multi-slice T2-weighted 2D imaging schemes making them impractical to use. The acquisition of images using saturation bands to form a reduced FOV (15.9 mm × 28.2 mm) and with 0.3 mm slices, but using a single slice package would have required 3 h per rat. If the images had been acquired in a single dataset with 0.15 mm thick slices, it would have required more than 6.5 h per rat. Alternatively, we could have acquired a dataset with an isotropic resolution of 0.15 mm using a 3D pulse sequence. The acquisition time for a single signal average would have been 3.3 h per rat if we had used saturation bands to reduce the FOV to 15.9 mm × 28.2 mm × 18 mm. However, it was not possible to use saturation bands with a 3D data acquisition scheme without unacceptable image wraparound artefacts and we would have had to use a FOV of 35 mm × 35 mm × 50 mm. This larger FOV would have resulted in an acquisition time of nearly 9.5 h to acquire data from one rat.

Construction of Ratlas-LH

The position of bregma in Ratlas-LH was defined as the position on the skull directly above the location where the anterior commissure crosses the midline of the brain (Paxinos et al., 1985); this was found to be aligned with the position of bregma as indicated by the micro-CT data when using the line of best fit (see Paxinos et al., 1985) once the MRI and micro-CT images were combined. The position of lambda is not so easily defined from in vivo MRI data. Furthermore, the lambdoid suture is less distinct in the anatomical average micro-CT template of the skull. This possibly reflects the variability of the intersection of the lambdoid and sagittal sutures (Paxinos et al., 1985), which may make the position of lambda less reliable for the derivation of stereotaxic coordinates.

A combination of signal averaging during MRI acquisition and the anatomical averaging of MRI datasets from seven rats provided a template with sufficient detail in three orthogonal planes for the purposes of determining in vivo coordinates for neurosurgical procedures. The ANTs template construction process has the advantage of providing an anatomical average template for the Lister hooded rat at this weight range, rather than relying on an exemplar image dataset to represent this age/weight group.

Use of Ratlas-LH

Ratlas-LH is available for free download (https://www.nitrc.org/projects/ratlas-lham). It was constructed from T2-weighted MRI and micro-CT images that were registered together. For those that are less familiar with MRI, it should be noted that in T2-weighted magnetic resonance images regions consisting of largely white matter appear dark grey compared to the rest of the brain and the ventricles appear white. The inclusion of the skull image data into the atlas means that coordinates for the implantation of devices can also be calculated relative to the skull surface.

It is worth noting that there were differences between the coordinate values that were successfully used for the implantations in the Lister hooded rat and those that would have been used based on the atlas of Paxinos and Watson (1998). This is particularly true for the cannula placements in the intermediate and ventral hippocampus and can be seen from the mappings of the infusion cannula placements on coronal sections from the atlas by Paxinos and Watson (1998) (Figures 5(c) and 7(c)), which are labelled with the distance from bregma as determined for the rats that were used for the construction of the Paxinos and Watson (1998) atlas. It is evident that the intermediate hippocampal cannulae placements are located in regions corresponding to 5.3–6.04 mm posterior to bregma in the Paxinos and Watson (1998) atlas (Figure 5(c)), whereas the coordinate derived from Ratlas-LH was 4.7 posterior from bregma. Moreover, the appropriate coordinate used for ventral hippocampal cannula placements in the Lister hooded rat was 5 mm posterior from bregma (McGarrity et al., 2017), whereas the placements centred around a region corresponding to a coordinate of about 6 mm posterior to bregma in the atlas of Paxinos and Watson (1998) (Figure 7(c)). This means that, for the hippocampal implants, coordinates chosen based solely on Paxinos and Watson (1998) would have been about 1 mm or more posterior to the coordinates determined based on Ratlas-LH, which would have resulted in many placements outside of the target regions in the hippocampus. For the placements in the medial nucleus accumbens, there was not a clear discrepancy between the anterior-posterior coordinate derived from Ratlas-LH (1.5 mm anterior from bregma) and the coordinate that would have been derived from Paxinos and

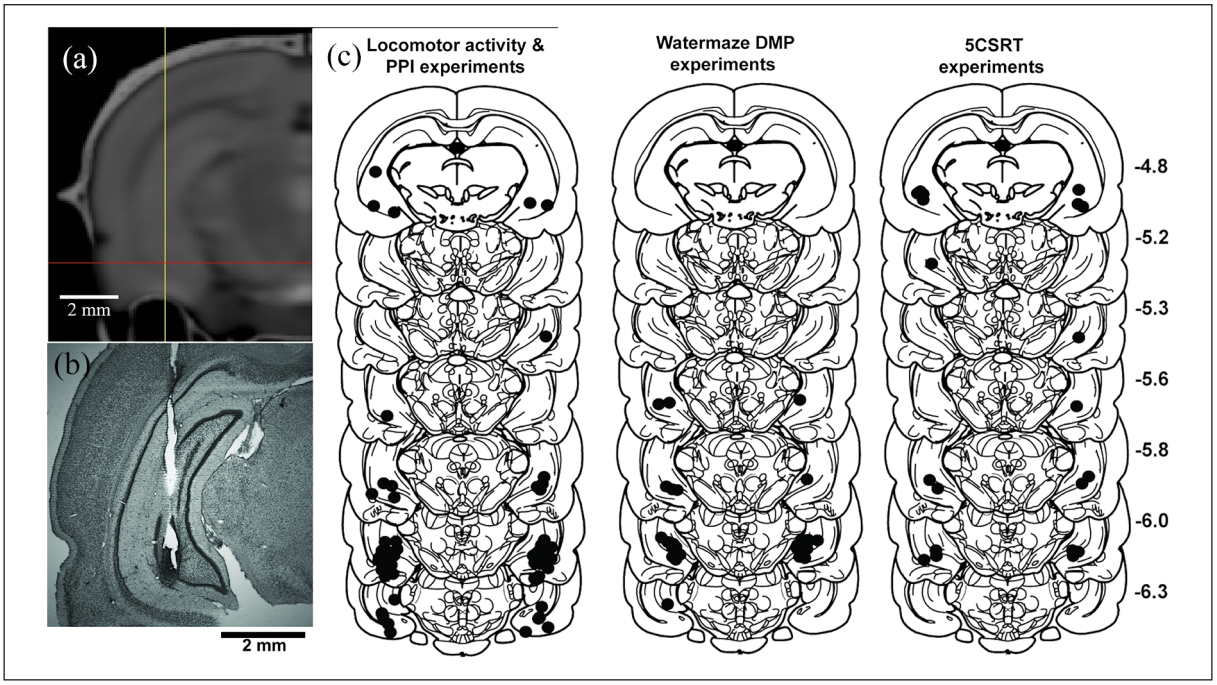

Figure 7. A comparison of the position in Ratlas-LH of the stereotaxic coordinates used by McGarrity et al. (2017) to target the ventral hippocampus and the infusion cannula placements in the ventral hippocampus that were achieved in McGarrity et al. (2017): (a) The position of empirically determined coordinates displayed in the Ratlas-LH (indicated by the red and yellow crosshairs in the image). (b) A photomicrograph of an example infusions site in McGarrity et al. (2017). (c) Spread of locations of infusion cannula tips (dots) across rats that received cannula implants targeting the ventral hippocampus in three different experiments from McGarrity et al. (2017). Locations are shown on coronal plates adapted from Paxinos and Watson (1998). Numbers indicate the distance (in mm) from bregma in the Paxinos and Watson (1998) coordinates system. (b) and (c) Reproduced from Figure 1(a) and (b), respectively, in McGarrity et al. (2017).

Watson (1998), with cannula placements located in regions corresponding to 0.48–2.7 mm anterior to bregma in the Paxinos and Watson (1998) atlas (Figure 6(c)).

Ratlas-LH does not replace the classic histological atlases (e.g. Swanson, 2004, or Paxinos and Watson, 2013) that provide high-quality detailed information on the structures within the rat brain. As described in the *Ratlas-LH validation 1: stereotaxic cannula implants using Ratlas-LH coordinate* section of the Methods, Ratlas-LH can be used alongside these classic atlases to determine stereotaxic coordinates for the Lister hooded rat brain by following the five-step process. Using a similar process, Ratlas-LH could be used to adjust, for use in Lister hooded rats, coordinates that have been reported in the literature for stereotaxic surgery in other rat strains. The delineations provided with Ratlas-LH are adapted from the WHS atlas of the Sprague Dawley rat brain (Kjonigsen et al., 2015; Osen et al., 2019; Papp et al., 2014) and can be displayed when using ITK-SNAP to view Ratlas-LH. The delineations are not as detailed as the delineation of the atlases of, for example, Paxinos and Watson (2013) and Swanson (2004), as they are based on multi-parametric MRI data and not histological information. However, they provide continuous 3D information of brain regions that can be viewed in any plane of Ratlas-LH and act as a guide to brain regions. When identifying regions of interest, we would recommend the use of a detailed atlas such as Paxinos and Watson (2013) or Swanson (2018).

Ratlas-LH may also prove useful for the display of data acquired from the Lister hooded rat, using functional imaging methods that do not generate a useful anatomical image, such as functional MRI (fMRI) or single photon emission computerised tomography (SPECT). In addition to the Ratlas-LH template, which includes brain MRI and skull micro-CT data, we have provided a brain-only template in the supplementary material, which may assist with the process of data registration and processing. The brain-only template and the full Ratlas-LH template occupy the same space, which means that any data fitted to the brain-only template can be displayed in Ratlas-LH. This also means that the delineations can be viewed on the brain-only template in ITK-SNAP and could be used to help identify regions of interest in fMRI or SPECT data.

Conclusion and future directions

The freely available Ratlas-LH may prove useful for experimental neuroscientists using the young adult male Lister hooded rat. In future, this resource could be expanded by the inclusion of Lister hooded rats of different age groups and for females as well as males. In addition, similar atlases could be generated for other commonly used rat and mouse strains. The anatomical detail of the atlas could be augmented by the inclusion of higher resolution ex vivo histological and MRI data.

Acknowledgements

We are grateful for access to the University of Nottingham's Augusta High Performance Computing service.

Declaration of conflicting interests

The author(s) declared no potential conflicts of interest with respect to the research, authorship and/or publication of this article.

Funding

The author(s) disclosed receipt of the following financial support for the research, authorship, and/or publication of this article: This project was supported by the University of Nottingham and a School of Psychology Pump-priming Award. S.M. was supported by a School of Psychology PhD studentship, G.H. by a School of Life Sciences PhD studentship and A.S. by a BBSRC DTP studentship. During preparation of this article, T.B. benefitted from a research sabbatical awarded by the School of Psychology, University of Nottingham.

ORCID iD

Malcolm J. W. Prior https://orcid.org/0000-0002-2123-9745

Supplemental material

Supplemental material for this article is available online.

References

Avants BB and Gee JC (2004) Geodesic estimation for large deformation anatomical shape averaging and interpolation. *NeuroImage* 23(Suppl. 1): S139–S150.

Avants BB, Tustison NJ, Song G, et al. (2011) A reproducible evaluation of ANTs similarity metric performance in brain image registration. *NeuroImage* 54(3): 2033–2044.

Hennig J, Nauerth A and Friedburg H (1986) RARE imaging: A fast imaging method for clinical MR. *Magnetic Resonance in Medicine* 3(6): 823–833.

Hess A, Hinz R, Keliris GA, et al. (2018) On the usage of brain Atlases in neuroimaging research. *Molecular Imaging and Biology* 20(5): 742–749.

Irani M and Peleg S (1990) Super resolution from image sequences. In: *Proceedings of the 10th international conference on pattern recognition*, Alantic City, NJ, 16–21 June, pp. 115–120. New York: IEEE.

Jenkinson M and Smith S (2001) A global optimisation method for robust affine registration of brain images. *Medical Image Analysis* 5(2): 143–156.

Jenkinson M, Bannister P, Brady M, et al. (2002) Improved optimization for the robust and accurate linear registration and motion correction of brain images. *NeuroImage* 17(2): 825–841.

Jenkinson M, Beckmann CF, Behrens TE, et al. (2012) FSL. *NeuroImage* 62(2): 782–790.

Kjonigsen LJ, Lillehaug S, Bjaalie JG, et al. (2015) Waxholm Space atlas of the rat brain hippocampal region: Three-dimensional delineations based on magnetic resonance and diffusion tensor imaging. *NeuroImage* 108: 441–449.

McGarrity S, Somerled S, Eaton C, et al. (2015) Medial prefrontal cortex is not required for, but can modulate, hippocampus-dependent behaviour based on rapid learning of changing goal locations on the watermaze delayed-matching-to-place test. *British Neuroscience Association Abstracts* 23: P1-D-013.

McGarrity S, Mason R, Fone KC, et al. (2017) Hippocampal neural disinhibition causes attentional and memory deficits. *Cerebral Cortex* 27(9): 4447–4462.

Osen KK, Imad J, Wennberg AE, et al. (2019) Waxholm Space atlas of the rat brain auditory system: Three-dimensional delineations based on structural and diffusion tensor magnetic resonance imaging. *NeuroImage* 199: 38–56.

Papp EA, Leergaard TB, Calabrese E, et al. (2014) Waxholm space atlas of the Sprague Dawley rat brain. *NeuroImage* 97: 374–386.

Paxinos G and Watson C (1982) *The Rat Brain in Stereotaxic Coordinates*. Sydney, NSW, Australia: Academic Press.

Paxinos G and Watson C (1986) *The Rat Brain in Stereotaxic Coordinates* (2nd edn). New York: Academic Press.

Paxinos G and Watson C (1998) *The Rat Brain in Stereotaxic Coordinates* (4th edn). San Diego, CA: Academic Press.

Paxinos G and Watson C (2013) *The Rat Brain in Stereotaxic Coordinates* (7th edn). Amsterdam: Academic Press.

Paxinos G, Watson C, Pennisi M, et al. (1985) Bregma, lambda and the interaural midpoint in stereotaxic surgery with rats of different sex, strain and weight. *Journal of Neuroscience Methods* 13(2): 139–143.

Pezze M, McGarrity S, Mason R, et al. (2014) Too little and too much: Hypoactivation and disinhibition of medial prefrontal cortex cause attentional deficits. *Journal of Neuroscience* 34(23): 7931–7946.

Pitiot A, Pausova Z, Prior M, et al. (2007) Magnetic resonance imaging as a tool for in vivo and ex vivo anatomical phenotyping in experimental genetic models. *Human Brain Mapping* 28(6): 555–566.

Seaton A (2019) *An investigation of the role of the nucleus accumbens in the hippocampal learning-behaviour translation*. PhD Thesis, University of Nottingham, Nottingham.

Simmons DM and Swanson LW (2009) Comparing histological data from different brains: Sources of error and strategies for minimizing them. *Brain Research Reviews* 60(2): 349–367.

Swanson LW (2004) *Brain Maps: Structure of the Rat Brain* (3rd edn). Amsterdam: Elsevier Academic press.

Swanson LW (2018) Brain maps 4.0-structure of the rat brain: An open access atlas with global nervous system nomenclature ontology and flatmaps. *Journal of Comparative Neurology* 526(6): 935–943.

Yushkevich PA, Piven J, Hazlett HC, et al. (2006) User-guided 3D active contour segmentation of anatomical structures: Significantly improved efficiency and reliability. *NeuroImage* 31(3): 1116–1128.

Zhang YY, Brady M and Smith S (2001) Segmentation of brain MR images through a hidden Markov random field model and the expectation-maximization algorithm. *IEEE Transactions on Medical Imaging* 20(1): 45–57.